

## Angularly resolved high-order harmonic generation in helium

J. W. G. Tisch, R. A. Smith, J. E. Muffett, M. Ciarrocca, J. P. Marangos, and M. H. R. Hutchinson

*The Blackett Laboratory, Imperial College, London SW7 2BZ, United Kingdom*

(Received 19 July 1993)

We report the observation of harmonics up to the 119th in helium, generated using a 1.053- $\mu\text{m}$ , 1-ps chirped-pulse-amplification laser at intensities up to  $3 \times 10^{14}$  W/cm<sup>2</sup>, and the measurement of their far-field spatial distribution. Complex spatial distributions are found for harmonics in the plateau region and near the cutoff; their angular distribution narrows to approximately that predicted by lowest-order perturbation theory.

PACS number(s): 42.65.Ky, 32.80.Rm

High-order harmonics of the fundamental frequency of laser radiation may be produced in the noble gases at laser intensities greater than  $10^{13}$  W/cm<sup>2</sup>. At sufficiently high intensities the distribution of the intensities of the harmonics with increasing harmonic order ( $q$ ) is characterized by a rapid decrease, followed by a plateau where, contrary to the predictions of simple lowest-order perturbation theory (LOPT), the efficiency of harmonic generation is not strongly dependent upon the order. At yet higher orders there is a relatively sharp decrease in efficiency to a cutoff, beyond which no harmonics are detected. In the plateau region, harmonics in the extreme ultraviolet (XUV) can be produced with brightness exceeding that obtainable from conventional sources, such as synchrotrons [1].

Theoretical studies of the interaction of high optical fields with atoms indicate that harmonics of order greater than 100 may be produced from atoms or ions with high ionization potentials [2,3]. In particular [3], it is suggested that the highest order of the harmonic may be determined by the maximum energy a free electron, born at rest in the optical field, can acquire. The maximum photon energy which it can emit as it oscillates in the field of the atomic core is

$$E_{\text{max}} \approx I_p + 3U_p.$$

$I_p$  is the ionization energy and  $U_p$  is the ponderomotive potential produced by the laser radiation and is given by

$$U_p = \frac{e^2 E^2}{4m\omega^2},$$

where  $E$  is the optical electric field and  $\omega$  is the optical frequency. For example, for a 1.053- $\mu\text{m}$  neodymium laser of intensity  $3 \times 10^{14}$  W/cm<sup>2</sup> with a target gas of helium ( $I_p = 24.6$  eV), the maximum harmonic order would be  $q \sim 100$ .

Experimental studies of high harmonic generation have been carried out at various laser wavelengths at intensities in the range  $10^{13}$ – $10^{17}$  W/cm<sup>2</sup> [4–8]. The highest-order process reported has been the 135th harmonic of 1.053- $\mu\text{m}$  radiation ( $\lambda = 7.8$  nm) [8] and the shortest wavelength (7.4 nm) obtained from the 109th harmonic of 806 nm Ti:sapphire laser radiation [6]. In addition to studies of the spectra of the harmonics, both the temporal [9,10] and spatial [9,11] distributions have been investigated. In such studies one must take into consideration not only the response of the atoms in the high field,

but also ionization, the resulting depletion of the neutral species, and the contributions to the phase matching from the atoms, ions, and free electrons.

We report the study of the angular distribution of the high harmonics in the region of the cutoff and show that the distribution narrows rapidly to a value consistent with LOPT as the cutoff is approached.

The laser used was a chirped-pulse-amplification (CPA) neodymium system in which pulses from a mode-locked Nd:YLF oscillator are passed through an optical fiber and a pair of expansion gratings. This combination stretches the pulse in time to 600 ps, increases the bandwidth to 4 nm, and imposes a frequency chirp. A single pulse is then selected for amplification in a Nd:glass regenerative amplifier to approximately 1 mJ and subsequently to  $\sim 1$  J in three additional rod amplifiers. Finally the pulse is compressed by a double pass through a grating pair to 1.3 ps, as measured by a single-shot autocorrelator. A small fraction of the beam is diverted to a calibrated calorimeter to provide a measurement of the pulse energy on each shot. The far-field profile of the amplified pulse has been measured by focusing the attenuated beam with a 5.2-m lens directly onto a charge-coupled device (CCD) array.

A schematic diagram of the experimental setup is shown in Fig. 1. The 35-mm-diam laser beam was focused into the helium gas jet to an intensity of  $\sim 3 \times 10^{14}$  W/cm<sup>2</sup> by a  $f = 1.7$  m plano-convex lens ( $f/50$ ) through a wedged antireflection coated window on the end of a vacuum extension tube. A long-focal-length lens was used for two reasons. First, for a given laser intensity in the focal plane, the harmonic signal scales as  $b^3$  [9] ( $b$  is the confocal parameter), and second, to minimize the effects of phase matching by operating in the loose focusing regime. The focal spot was elliptical and the confocal parameter was measured to be  $\sim 20$  mm by scanning the distribution in the focal plane of a long-focal-length lens. The Mach 5 pulsed solenoid-valve gas jet was backed with 40 atm of helium, the supersonic flow ensuring that the interaction zone was free of shock waves which could modify the spatial profile of the harmonics. The gas distribution had a width of  $\sim 1$  mm with a number density of  $\sim 10^{17}$ /cm<sup>3</sup>.

A grazing-incidence (87°) flat-field spectrometer [12] was used to disperse the harmonics which propagate collinearly with the laser beam. The entrance slit was 50  $\mu\text{m}$

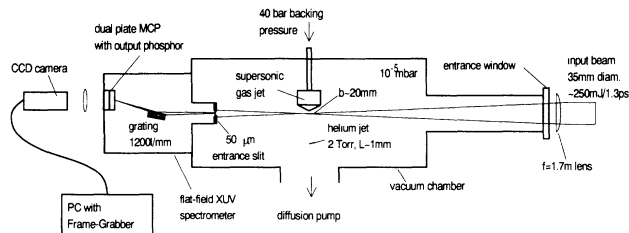


FIG. 1. Schematic diagram of the experimental layout.

wide and 15 mm long and provided a spectral resolution of 0.05 nm in the region of interest. The spectrometer was placed 600 mm from the laser focus and the laser pulse energy was limited to less than 400 mJ to prevent damage to the slit of the spectrometer.

A gold-coated  $50 \times 30\text{-mm}^2$  concave grating of 5649 mm radius-of-curvature and of variable pitch (approximately 1200 1/mm) was used to produce an aberration-corrected, flat focal field. The distances from the grating center to the entrance slit and the image plane were 235 and 237 mm, respectively. In the focal plane, the reciprocal dispersion varied from 0.43 to 0.77 nm/mm over the wavelength range 5–20 nm. Spectra were recorded with a double-plate MCP of  $50\text{-}\mu\text{m}$  resolution, sensitized for the XUV with CsI, which was placed close to the focal plane of the spectrometer. Although the operating range of the spectrometer was 3–30 nm, the aperture of the detector limited the range to 12 nm for a single laser shot. The output phosphor of the multichannel plate (MCP) was coupled to an intensified CCD camera and the images analyzed with a personal computer and frame-grabber system. The overall gain of the detection system was  $\sim 10^8$ .

The spectrometer was calibrated spectrally by three independent methods. First, a split-field filter comprising 150 nm thickness of aluminum and 100 nm of Formvar (a carbon-rich plastic) was positioned behind the entrance slit, which was illuminated by continuum radiation from a laser-irradiated copper target. The cutoffs at the carbon *K*-shell absorption edge at 4.4 nm and the aluminum *L*-shell absorption edge at 17.3 nm provide calibration wavelengths. Second, the harmonics transmitted by the Al section of the filter were monitored and the highest order ( $q = 61$ ) transmitted by the filter identified. Third, recombination lines from solid targets (carbon, boron, and LiF) placed in the laser focus were recorded. The results of these calibration techniques together with the measured harmonic wavelengths over the range 6–15 nm are shown in Fig. 2.

Since one of the aims of the experiment was to study the angular dependence of the harmonics, the spatial imaging properties of the spectrometer and detection system were of importance. Figure 3 shows the image observed in the exit plane of the continuum radiation from a copper target when the combination Formvar and Al filter is placed close to the entrance slit, partially covering the field. The linearity of the (spatial) edge of the sections of the spectrum recorded through the different filters confirms the fidelity of the image in the spatial dimension orthogonal to the direction of dispersion. The separation of the spectrometer ( $\gg b$ ) from the interaction region

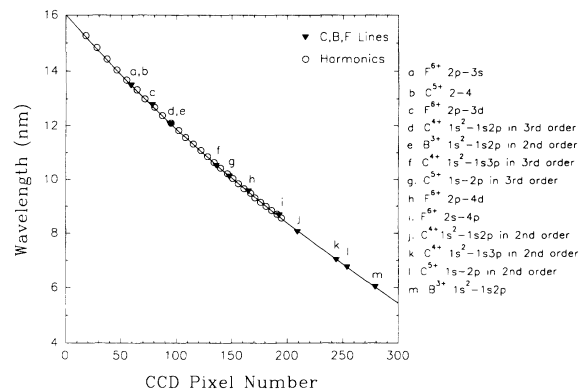


FIG. 2. Calibration curve for the spectrometer ( $\blacktriangledown$ , recombination lines from solid targets;  $\circ$ , harmonics).

was sufficient to ensure that the angular distribution of the harmonics was measured in the far field.

In Fig. 4 we present a harmonic spectrum that was obtained by averaging spectra from 18 shots of similar intensity. The highest reliably identified harmonic is  $q = 119$ . The intensity scale is not absolute, since the wavelength dependence of the throughput and sensitivity of the detection system have not been accurately determined. However, from solid target emission spectra it is known that the MCP detector is sensitive down to 4 nm and that its gain is relatively flat over the range 5–20 nm. The observed cutoff around  $q = 117$  is therefore believed to be real and not a detection artefact. Insertion of a  $\lambda/4$  retardation plate in the laser beam, before the focusing lens, completely eliminated the signal and confirmed that the short-wavelength radiation was indeed produced by harmonic generation, since harmonic generation is prohibited using circularly polarized laser radiation because of angular momentum conservation.

The maximum efficiency of harmonic generation was estimated from the fact that the harmonic energy from 100 laser shots was insufficient to expose Kodak 104 x-ray film. Assuming a sensitivity of  $\sim 1$  photon/ $\mu\text{m}^2$  [13] and a uniformly illuminated area of film of  $\sim 2.5$  mm  $\times$  0.2 mm =  $5 \times 10^5$   $\mu\text{m}^2$ , this implies that fewer than 5000 photons were incident on the film per shot. Taking into account the collection geometry, this corresponds to the generation of  $\lesssim 10^6$  harmonic photons per pulse and, at a laser pulse energy of  $\sim 200$  mJ ( $10^{18}$  photons), a con-

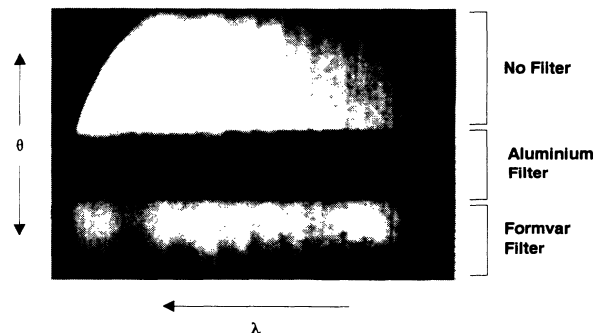


FIG. 3. Spatial image of the split filter illuminated with continuum radiation from the Cu target.

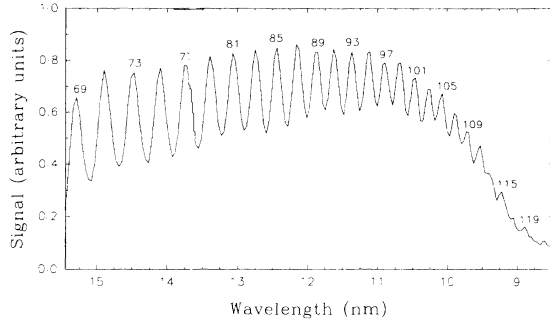


FIG. 4. Measured spectrum of high harmonics in helium (uncorrected for the sensitivity of the spectrometer and detection system).

version efficiency less than  $10^{-12}$ .

The spatial structure of a typical harmonic spectrum is shown in Fig. 5. It consists of a number of closely spaced harmonics starting in this example at  $q = 69$ . The lower harmonics are partially obscured by the circular aperture of the MCP detector, but there is a marked and rapid decrease in the angular divergence with increasing  $q$ , pinching down to a cutoff, in this case at around  $q = 115$ . This spatial collapse was observed to be associated with the approach of the cutoff in the harmonic order over the range of laser intensities studied ( $\sim \times 3$ ).

Although LOPT theory is known to be inadequate for strong field interactions, it is instructive to reiterate its predictions in the weak-field limit where, for constant phase mismatch ( $\Delta k$ ), the intensity of the  $q$ th harmonic is proportional to the  $q$ th power of the laser intensity. For a Gaussian laser beam, the far-field intensity angular distribution can be written as

$$I(\theta) \propto \exp \left\{ -2 \left[ \frac{\theta}{\theta_0} \right]^2 \right\},$$

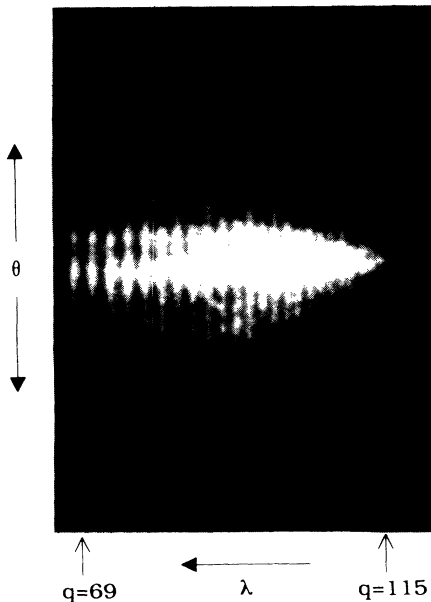


FIG. 5. Spatially and spectrally resolved harmonic spectra in the region of the cutoff.

and the harmonic intensity would be given by

$$I_q(\theta) \propto \exp \left\{ -2 \left[ \frac{\theta}{\theta_0 q^{-1/2}} \right]^2 \right\},$$

with the cone angle decreasing relatively weakly with harmonic order as  $q^{-1/2}$ .

The angular distributions of four harmonics ( $q = 71, 91, 101, \text{ and } 111$ ) are shown in Fig. 6. The peak heights have been normalized to ease comparison. The dashed curve is the distribution predicted by LOPT. The laser intensity distribution in the focal plane was approximately Gaussian in the direction parallel to the slit, with  $\theta_0 \sim 10$  mrad. From Fig. 6 it can be seen that the 71st harmonic displays considerable structure. With increasing harmonic order, the structure decreases in width, increases in intensity, and merges with the central peak to produce a distribution which is approximately Gaussian. As the cutoff is approached, the distributions narrow and approach those predicted by LOPT.

The angular distribution of the harmonics is governed both by the atomic response and propagation through the ionizing medium. The dipole moment at the harmonic frequency  $d(\omega_q)$  and the rate of photoionization may be computed by time-dependent numerical solution of the Schrödinger equation for the atom in the intense field [9,14]. These show that, at relatively low intensities, the magnitudes of the dipoles increase rapidly with intensity, but flatten and show oscillations at high intensities due to intensity-dependent resonances. This change in behavior characterizes the onset of the plateau. In a given intensity range, the harmonics in the plateau have already at

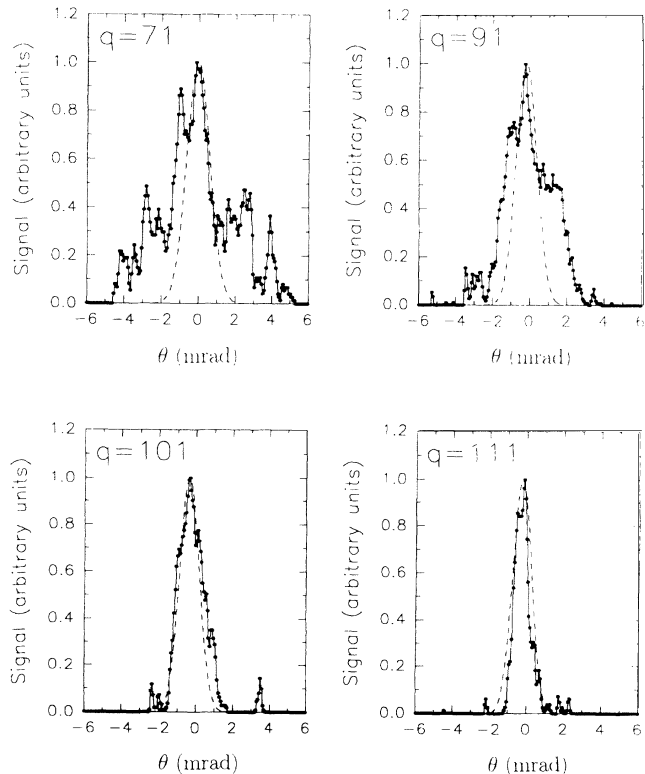


FIG. 6. Spatial profiles of harmonics (dashed line is distribution predicted by LOPT).

tained this saturated intensity dependence, whereas the dipoles associated with the higher-order harmonics near the cutoff still are strong, monotonic functions of intensity.

The spatial distribution of the source of a given harmonic is governed by this intensity-dependent behavior of the dipole moment. Thus, for the plateau harmonics, the spatial distribution of the intensity which is proportional to  $|d(\omega_q)|^2$  will be broad with a complex structure (due to resonances) that deviates significantly from the Gaussian profile of the input laser field, while for the harmonics near the cutoff, it will be concentrated around the optical axis with essentially a Gaussian form comparable to that expected for LOPT.

The propagation of these harmonics is strongly influenced by the dispersion of the free electrons produced by photoionization of the medium. The free-electron phase mismatch is

$$\Delta k = k_q - qk_1 = \omega_p^2(q^2 - 1)/2qc\omega,$$

where  $\omega_p$  is the plasma frequency of the ionized gas. This is much larger than that of the atomic or ionic species when the degree of ionization is high. Since the harmonics near the cutoff are generated very near the optical axis where the radial gradient of the electron density is low,

the change in phase across the harmonic beam is relatively small. However, the plateau harmonics are generated in a region which extends to much larger radii where the gradient of the electron density distribution and hence the variation in phase are significantly larger. As a result, although propagation of the plateau harmonics is strongly modified by free-electron dispersion, giving rise to broadening far-field distributions with complex structure, the highest harmonics are less affected and propagate as near Gaussian beams, giving distributions with low divergence.

In summary, we have shown that the spatial structure of very high harmonics depends strongly on the harmonic order in the region of the cutoff, approaching that predicted by lowest-order perturbation theory, and have suggested a possible explanation for this behavior in terms of the intensity dependence of the components of the single-atom dipole moment.

We wish to thank P. L. Knight, O. Willi, and S. Augst for helpful discussions and the Rutherford Appleton Laboratory for the loan of the flat-field spectrometer. Financial support by the Science and Engineering Research Council is gratefully acknowledged.

- 
- [1] X. F. Li, A. L'Huillier, M. Ferray, L. Lompre, and G. Mainfray, *Phys. Rev. A* **39**, 5751 (1989).
  - [2] K. Burnett, V. C. Reed, and P. L. Knight, *J. Phys. B* **26**, 561 (1993).
  - [3] J. L. Krause, K. J. Schafer, and K. C. Kulander, *Phys. Rev. Lett.* **68**, 3535 (1992).
  - [4] N. Sarakura, K. Hata, T. Adachi, R. Nodomi, M. Watanabe, and S. Watanabe, *Phys. Rev. A* **43**, 1669 (1991).
  - [5] K. Miyazaki and H. Sakai, *J. Phys. B* **25**, L83 (1992).
  - [6] J. J. Maklin, J. D. Kmetec, and G. L. Gordon III, *Phys. Rev. Lett.* **70**, 766 (1993).
  - [7] J. K. Crane, M. D. Perry, S. Herman, and R. W. Falcone, *Opt. Lett.* **17**, 1256 (1992).
  - [8] A. L'Huillier and P. Balcou, *Phys. Rev. Lett.* **70**, 774 (1993).
  - [9] A. L'Huillier, K. J. Schafer, and K. C. Kulander, *J. Phys. B* **24**, 3315 (1991).
  - [10] M. E. Faldon, M. H. R. Hutchinson, J. P. Marangos, J. E. Muffett, R. A. Smith, J. W. G. Tisch, and C-G. Wahlström, *J. Opt. Soc. Am. B* **9**, 2094 (1992).
  - [11] D. D. Meyerhofer and J. Peatross (private communication).
  - [12] N. Nakano, H. Kuroda, T. Kita, and T. Harada, *Appl. Opt.* **23**, 2386 (1984).
  - [13] J. Krishnan, D. Neely, C. Danson, L. Dwivedi, C. L. S. Lewis, and G. J. Tallents, SERC Rutherford Appleton Laboratory CLF Annual Report No. 22, 1992 (unpublished).
  - [14] J. L. Krause, K. J. Schafer, and K. C. Kulander, *Phys. Rev. A* **45**, 4998 (1992).

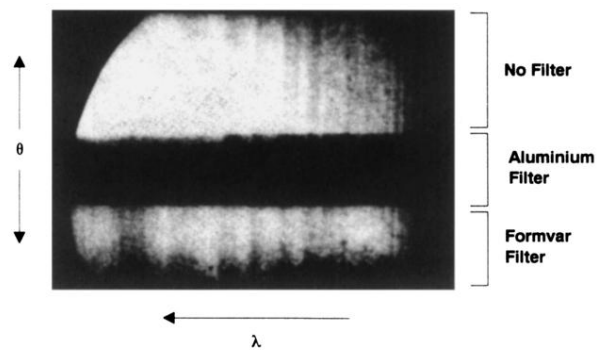


FIG. 3. Spatial image of the split filter illuminated with continuum radiation from the Cu target.

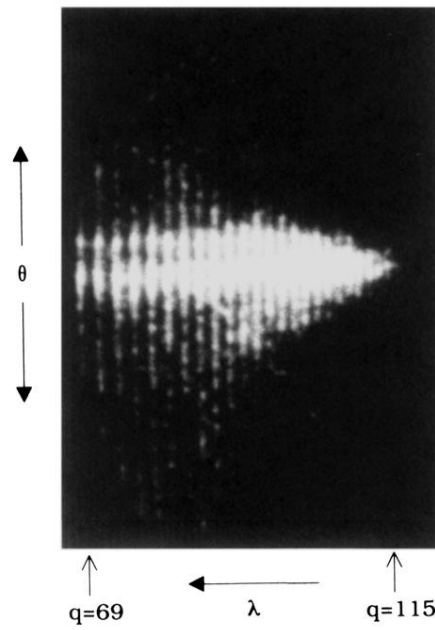


FIG. 5. Spatially and spectrally resolved harmonic spectra in the region of the cutoff.